An improved model for predicting liquid loading onset in inclined pipes with non-uniform liquid wall films

Abstract

Liquid loading is a phenomenon in which liquid accumulates in the wellbore of mature gas wells, causing a significant reduction in production and sometimes permanent well abandonment. This paper introduces a new model for predicting liquid loading onset, based on the reversal of a non-uniform liquid film. The momentum balance equation for annular flow is, in the proposed model, expressed as a function of liquid holdup instead of liquid thickness. The model employs auxiliary correlations to obtain liquid holdup and an interfacial friction factor, developed from literature data.

The accuracy of the proposed model is quantified by comparing laboratory data from this work and field datasets from previous studies, with the predictions of existing models. The proposed model successfully reproduces the experimental data and field data, and gives the highest prediction accuracy and the lowest average error when compared with existing models. The proposed model therefore represents a significant improvement on existing models.

The applicability of auxiliary correlations means that this model should be restricted to upward pipe inclinations of 30° to 90° from the horizontal, liquid viscosities of 1.1cP and 0.018 cP, and superficial velocities of gas of 3-60 m/s and of liquid of 0.01-0.2m/s. Results show that the model exhibits poor performance when applied to pipe inclinations lower than 30° from the horizontal.

Keywords

Inclined pipe
Critical gas velocity
Two-phase flow
Liquid loading onset
New model

1. Introduction

Natural gas production is, due to the environmental footprint being smaller than for oil and coal production, becoming more and more attractive. Advances in engineering practices and the discovery of large offshore gas fields has further increased oil company interest in developing projects in unconventional gas fields.

Exploration in deep-water and the development of horizontal wells has led to the high range of deviated production wells we see today, these ranging between 10º and 85º of inclination. These inclinations have an enormous effect on the fluid flow of multiphase flows in production strings. Moderate amounts of liquid, such as condensate and water, are also produced in gas wells. These are the result of condensate dropout due to pressure and temperature reductions or of water breakthrough, the liquids produced accumulates in the wellbore due to the liquid fraction increasing or gas rates decreasing (e.g. with depletion). The ability of the flow to carry these liquids to the surface is therefore lost, a phenomenon known as liquid loading. This can cause further reductions in gas rates due to excessive back-pressure on the formation and erratic production. The ability to accurately predict the onset of liquid loading is therefore an essential factor in effective gas well planning and design. Little has been published on liquid loading onset in inclined wells, most correlations having been developed for vertical wells, this having a limited applicability to inclined wells. The prediction of liquid loading onset in inclined gas wells is an area in which there is a great need for more knowledge.

Gas flow rates in early production stages are high enough to carry co-produced liquids out of the well. Well production conditions are therefore stable (annular flow regime). Gas production rates drop in later stages of a well's life, as reservoir pressure falls. The capacity to lift any liquid to the surface therefore approaches and ultimately becomes zero when below a critical gas rate. Liquids present in the wellbore, where flow falls below the critical gas rate, therefore start to flow in the opposite direction. Intermittent flow patterns then can develop in some parts of the tubing, leading to an unstable production condition. Non-removed liquid accumulates under these conditions in the wellbore, leading to a phenomenon commonly known as liquid loading. The accumulated liquid creates a backpressure on the formation, increased resistance along the gas production pathway, further accumulation of liquid, a reduction in the natural flow of gas from the reservoir to the surface, and eventually the premature abandonment of the well. This leads to financial losses due to the early curtailment of hydrocarbon sales and to higher operational costs.

Co-produced fluids can be free liquid that flows with the gas from the reservoir. They can also be condensate and water that separate out from the gas due to pressure and temperature reductions along the tubing. Irrespective of their origin, these fluids are either entrained as droplets in the gas core and/or occur as a film attached to and that moves along the pipe wall. Fig. 1-1 illustrates how a gas well can behave over time as reservoir pressure falls.

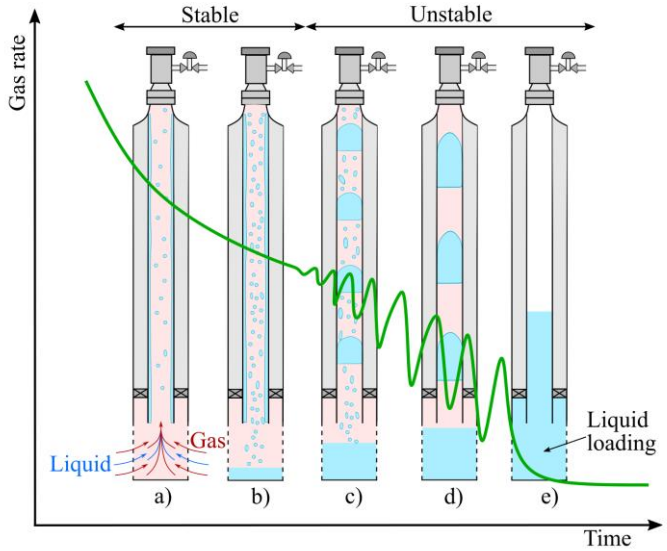

Fig. 1-1 Production profile for gas wells experiencing liquid loading. Adapted from Fernandez et al. (2010).

Deliquification methods such as gas lift, plunger lift, production cycling, and down-hole pumps are often installed in wells to counteract liquid loading, and to maintain production. Operators must, however, be able to accurately predict the onset of liquid loading, so that deliquification methods are deployed early enough to prevent premature well shut-in.

A number of researchers (Vitter, 1942; Jones, 1946; Duggan, 1961 cited by Turner et al., 1969; Guo et al., 2005 and Chupin et al., 2007) have proposed methods for determining the onset of liquid loading. These methods typically are based on the correlation of field and experimental data, on equations derived from mechanistic models or a combination of the two. Almost all of these studies agree, however, on two physical models for the removal of liquid in gas wells (see Fig. 1-2): (a) liquid is transported as droplets entrained in the high velocity gas core and (b) liquid is transported as a film that moves along the pipe walls.

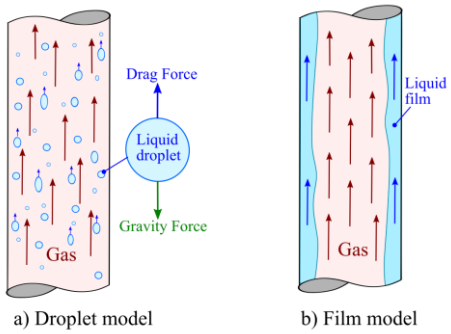

Fig. 1-2 Illustrative diagram of liquid transportation in gas well, Fernandez et al. (2010).

1.1 Liquid droplet model

The entrained liquid droplet model, also known as liquid droplet reversal, assumes that the main cause of liquid loading is the falling backwards of liquid droplets held in the gas core. Turner et al. (1969) proposed an equation for calculating the minimum gas velocity required to lift the largest droplet present in a gas core, liquid loading being therefore likely when the gas velocity in the tubing drops below this minimum gas velocity. Turner's equation for critical superficial gas velocity (m/s) is based on the drag and gravity forces that act on a falling liquid droplet, and therefore is:

$$v_{\mathrm{sg,critical}} = 6.556\left[\frac{g(\rho_l - \rho_g)\sigma}{\rho_g^2}\right]^{0.25} \quad 1\text{-}1$$

The original coefficient of 5.463 was, however, changed to 6.556 (a 20% correction) to match the equation results with the field data Turner et al. used in model validation.

Many researchers have, to varying degrees of success, refined and modified the Turner et al. (1969) droplet model to achieve a better match between the equation and different data sets (Coleman et al., 1991; Nosseir et al., 1997; Li et al., 2001; Wang et al., 2010 and Sutton et al., 2010). Modifications address aspects such as liquid droplet shape, equation coefficient values and the effect of flow conditions.

Turner et al.'s equation has, however, been widely used in the petroleum industry as the primary method for predicting liquid loading in gas wells. The quickly increasing need to predict liquid loading in inclined wells has led to the droplet model being modified to include the effect of inclination. Flores-Avila et al. (2002) proposed a new droplet model based on the Turner et al. model, by adapting the model to field units and by including a coefficient to account for well inclination angle.

Belfroid et al. (2008) studied the effect of pipe inclination angle on droplet model prediction, plotting critical gas velocity as a function of inclination angle using data from van 't Westende et al. (2007), as shown in Fig. 1-3. The plot shows critical gas velocity increasing to a maximum value as inclination angle moves away from the vertical, and then dropping away as inclination angle increases beyond this.

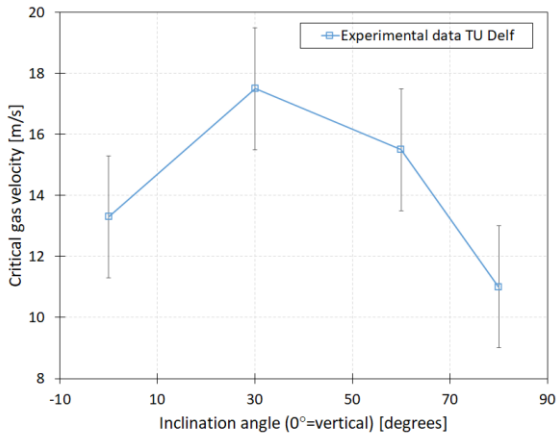

Fig. 1-3 Critical gas velocity vs. inclination angle (Belfroid et al., 2008)

This behaviour was attributed to the decrease in gravitational force perpendicular to the flow and the increase in film thickness along the full circumference of the tubing. Belfroid et al. furthermore proposed a new droplet model that can account for the effect of inclination angle on critical gas velocity prediction through combining the Fiedler et al. (2004) model with the conventional Turner equation. Belfroid's equation for critical superficial gas velocity (m/s) therefore is:

$$\dot{m}_{g,min} = \left(3.1\mathrm{A}\sqrt{\rho_g}\right)\left[g\sigma(\rho_l - \rho_g)\right]^{0.25}\frac{(\sin 1.7\theta)^{0.38}}{0.74} \quad 1\text{-}2$$

where $\dot{m}_{g,min}$ is minimum gas mass flow rate [kg/s], ρ_g gas and ρ_l liquid density [kg/m^3], σ surface tension [N/m] and θ inclination angle in relation to the horizontal (where θ = 0°).

Wang et al. (2016) subsequently conducted an experimental study of an air-water flow system in coiled pipes, with inner diameters of 30 mm and 40 mm, and inclinations of 15° to 76° from the horizontal. Based on their experimental data, they proposed a modification to the Belfroid et al. (2008) model to include the effect of pipe diameter on the prediction of critical gas velocity.

Some field and experimental evidence has shown that the predictability of the droplet model, which is otherwise simple, easy to use and to tune, is however limited (Guo et al., 2005;Veeken et al., 2010; Shekhar et al., 2017; Vieira et al., 2019a; Vieira et al., 2019b).

1.2 Liquid film model

The liquid film model, which is also known as the liquid-film-reversal model, assumes that liquid is transported as a film along the walls of the conduit, the gas core flowing on the inside of this. Liquid starts to accumulate in wells when the liquid film can no longer be lifted to the surface. Turner et al. (1969), based on field data analysis, however concluded that the liquid film is not the controlling liquid transport mechanism. An approach based on pressure gradient and flow regime transitions was therefore proposed to identify when the liquid film can no longer be lifted to the surface.

Zabaras et al. (1986) conducted an experimental study of the film flow of a vertically upwards concurrent annular gas-liquid flow, measuring instantaneous local film thickness, wall shear stress and pressure gradient. They concluded that film motion is, at low gas flow rates, controlled by a switching mechanism which they designated churn flow, which is linked to the instability of the liquid film due to decreasing film-thickness and interfacial friction. A number of authors have subsequently also shown that liquid loading is accompanied by a flow regime transition from annular flow to slug or churn flow (intermittent flow), the annular-intermittent transition model of Barnea (1986 , 1987) being therefore widely used to determine the onset of liquid loading in inclined pipes. This model assumes no variation in film thickness around the pipe at all inclination angles, and that the transition from annular to intermittent flow takes place where the gas core is blocked by the liquid, so leading to slug flow. This blockage is due to two mechanisms: (a) the instability of the annular flow configuration and (b) spontaneous blockage of the core due to wave growth on the liquid film.

Paz (1994) conducted an experimental and theoretical investigation into two-phase annular flow, the focus of this study being the effect of inclination angle on liquid film thickness distribution along the circumference of the pipe. They observed that the liquid phase tends to accumulate at the bottom of the pipe as pipe inclination approaches horizontal. This results in a thicker liquid film at the bottom and a thinner film at the top of the pipe (Fig. 1-4). They therefore concluded that inclination angle strongly affects liquid film thickness (δ), so proving Barnea's assumption to be incorrect.

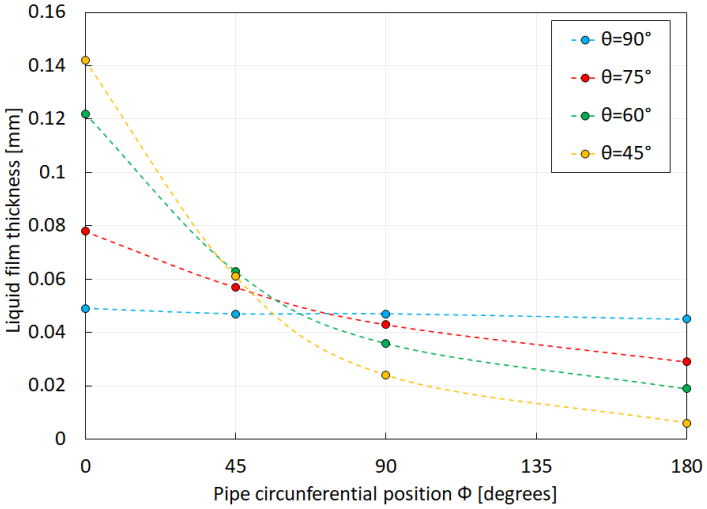

Fig. 1-4 Liquid film thickness distribution around the pipe circumference (φ = 0° at the bottom of the pipe) for v_{sg}=18.29 m/s, v_{sl}=0.0124 m/s, different pipe inclination (θ=90° is vertical) observed by Paz (1994)

Luo et al. (2014) subsequently published a correlation that took into account non-uniform film thickness (Equation 1-6) and used Barnea's (1986) methodology to predict the onset of liquid loading. I.e. annular-intermittent transition and Fore et al.s' (2000) interfacial friction factor correlation (Equation 1-3) instead of Wallis' (1969).

$$f_i = 0.005\left\{1 + 300\left[\left(1 + \frac{17500}{Re_g}\right)\tilde{\delta}_L - 0.0015\right]\right\} \qquad 1\text{-}3$$

The new correlation was developed by comparing a uniform and non-uniform film thickness model, as shown in Fig. 1-5. The area of the film where film thickness is uniform was approximated to the area of an expanded rectangle, and to a trapezoid (see Equation 1-4) for non-uniform film thickness as used by Barnea (1986).

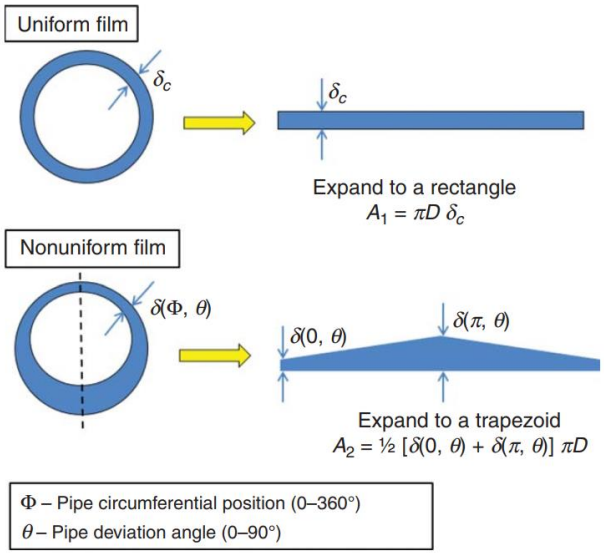

Fig. 1-5 Schematic of uniform and non-uniform liquid film thickness. Taken from Luo et al. (2014).

$$A_1 = \pi D \delta_c \qquad A_2 = \frac{1}{2}[\delta(0,\theta) + \delta(\pi,\theta)]\pi D \tag{1-4}$$

where D is pipe diameter, δ_c is constant film thickness, $\delta(0,\theta)$ is film thickness at the top of the pipe and $\delta(\pi,\theta)$ is film thickness at the bottom of the pipe. If $A_1 = A_2$, then constant film thickness can be expressed as

$$\delta_c = \frac{1}{2}[\delta(0,\theta) + \delta(\pi,\theta)] \tag{1-5}$$

Luo et al. proposed the following empirical equation for film distribution along the pipe circumferential position for different pipe deviations

$$\delta(\varphi,\theta) = (1 - \alpha\theta\cos\varphi)\delta_c$$
$$\alpha = \begin{cases} 0.0287 & 0 \le \theta < 30 \\ 0.55\theta^{-0.868} & 30 \le \theta \le 90 \end{cases} \tag{1-6}$$

The equation was developed from a simple curve fitting of Paz (1994) data, the ratio between the minimum (thickness at top of the pipe) and the maximum film thickness measure being plotted against the pipe inclination angle for each liquid velocity.

The critical film thickness ($\tilde{\delta}_L$) was calculated by differentiating the combined momentum equation, which was then converted to an equivalent film thickness (δ_c). This allows the equation for the variation of film thickness due to pipe inclination to be incorporated into the prediction of onset of liquid loading. The equivalent film thickness was then used to calculate the critical gas velocity for an inclined pipe, by applying the methodology proposed by Barnea (1986).

Shekhar et al. (2017) subsequently proposed a new set of empirical correlations using this concept of film thickness variation with pipe inclination (Equation 1-7), and the criterion developed by Barnea (1986). They, however, assumed that liquid loading onset in an inclined pipe would begin when the liquid film at the bottom of the pipe starts falling back.

$$\delta(\varphi,\theta) = \left[1 - \left(\frac{1 - e^{-0.088\theta}}{1 + e^{-0.088\theta}}\right)\cos\theta\right]\tilde{\delta}_{avgL} \tag{1-7}$$

They, to calculate the critical gas velocity, estimated the maximum film thickness for the required shear stress using Equation 3-1, and then converted the film thickness using the relation given in Equation 1-8. Their corrected $\tilde{\delta}_{avgL}$ was then substituted back into the Barnea (1986) Equation 3-1, to determine the critical superficial gas velocity.

$$\tilde{\delta}_{avgL} = \frac{1}{2}\left(1 + e^{-0.088\theta}\right)\tilde{\delta}_{max} \tag{1-8}$$

They also modified the Wallis (1969) interfacial friction faction (f_i) and proposed a correlation that is dependent on the inclination angle (Equation 1-9).

$$f_i = 0.005\{1 + [340(1 + \cos\theta)\tilde{\delta}_{avgL}]\} \quad 1\text{-}9$$

The new model was validated using data from Alsaadi (2013) and Guner (2012), and shows an improvement in the prediction of onset of liquid loading.

The nodal analysis concept was also taken as a new criterion for predicting the onset of liquid loading. This analysis concept suggests that liquid starts to accumulate at the wellbore when the pressure in the production tubing decreases to a minimum pressure.

Zabaras et al. (1986) observed, through experimental data, that pressure drop displays a minimum as the gas flow rate is reduced for a given constant liquid flow rate. This pressure drop behaviour was accompanied by the annular-intermittent flow transition. Researchers such as Kelkar et al. (2013), Sarica et al. (2013), Luo et al. (2014) and Waltrich et al. (2015) subsequently started to use the concept of minimum pressure to define the initiation of liquid loading.

Such methods have been shown to be useful in the prediction of the onset of liquid loading for experimental and in some cases field data. Model improvement is, however, required to account for the pipe inclination effect in gas wells.

1.3 Problem statement and methodology

The objective of this work is to develop a more accurate model to predict the onset of liquid loading in inclined pipes, for non-uniform liquid film. The model is based on the Barnea (1986) model, most terms being expressed for liquid holdup instead of equations being expressed as a function of liquid film thickness, as used in most previous work (e.g. Barnea and Shekhar). Auxiliary correlations were developed using the experimental data presented by Paz (1994).

The model was validated using experimental gas-liquid flow data in an inclined pipe collected by the authors at an experimental facility. Pipe diameter was 60 mm, length was 7 m and inclinations were 20° to 78° upwards. The model was also compared with the models of Shekhar et al. (2017) and Barnea (1986). Model accuracy was quantified.

The model was validated against field data reported in previous work by Turner et al. (1969), Belfroid et al. (2008) and Veeken et al. (2010), and compared against the output of the models of Shekhar and Barnea. Modifications are suggested to improve the accuracy of the new model. Model accuracy was quantified.

2. Experimental facility

Experiments were performed at the multiphase flow laboratory at NTNU as an extension of the work reported by Vieira et al. (2019a) and Vieira et al. (2019b). The test section consists of a transparent acrylic pipe of 60 mm inner diameter and length of approximately 7 m, resting on a steel beam connected to a lift mechanism. The lift mechanism allows the section to be easily adjusted to a predefined inclination angle on the beam, using a connected lift handle. Test section inclination ranged from 0° to 90° (to the horizontal). Inclination angle was, however, limited by the structure supporting the steel beam having a maximum predetermined inclination of 78° due to safety when performing experiments with velocities above 20m/s. The lift system allowed the test section to be adjusted to angles between the horizontal and vertical. A schematic of the test section is shown in Fig. 2-1.

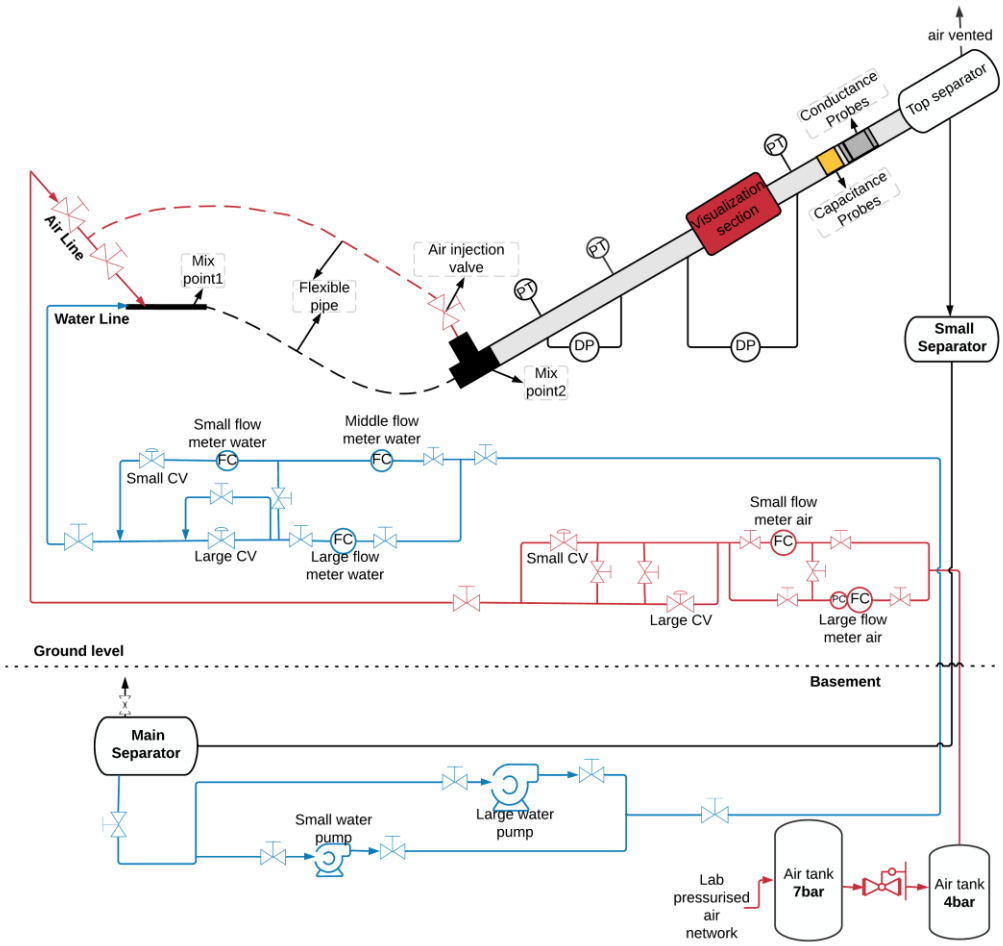

Fig. 2-1 Schematic of inclined test section at multiphase flow loop at NTNU

The inclined facility has two locations to mix the test fluids. Mixpoint2 (Fig. 2-1) was, however, used in this work to avoid instabilities caused by the flexible pipe. The two-phase propagates, after the mixing point, through the test section to a separator located at the top of the pipe. The phases are separated here, the gas phase being discharged to the atmosphere and the liquid being sent back to a storage tank in the basement. Water and compressed air were used as test fluids, and a ball valve was used to control gas injection in the test section. Air was supplied at 7 bar, stored in the air buffer, and then reduced to the experimental conditions of 4 bar. The water was pumped from the storage tank to the test section by centrifugal pumps. Air flow rate was measured by a Vortex flow meter and the water flow rate by a Coriolis flow meter. The fluid properties under test conditions, i.e. 20°C and 1 atm are given in Table 2-1.

Table 2-1 Liquid and gas properties @ 20 °C, 1bar

Fluid	Density [kg/m^3]	Viscosity [cP]	Surface tension [mN/m]
Water	997.9	1.1	60
Air	1.2	0.018	-

Instrumentation was installed in the test section, the pressure gradient being measured by two differential pressure cells and three absolute pressure sensors. The range of the differential pressure cells were ±50 kPa and ±64 kPa, and the range of the absolute pressure sensor was 0-200kPa.

Calibration was carried out every day before experiments were conducted, to ensure acceptable pressure drop measurement accuracy. Conductance probe rings were installed at the end of the pipe and liquid holdup was determined through a voltage signal conversion using a calibration curve.

A high-speed camera (GoPro Hero 6 Black®) was installed and used to identify the onset of liquid loading. Pictures and videos were recorded at a *visualization section* approximately 4 m above the test section entrance. Fluctuation signals from pressure sensor and conductance probe rings were also used to additionally support the identification of the critical gas velocity. Fig. 2-2, for example, shows the pressure gradient from the differential pressure cell located 1.35 m above the test

section injection mix point 2 and the conductance probe signal, for a time period in which the gas rate was reduced in three steps. Both signals fluctuate when the fluid transitions to slug flow pattern occur.

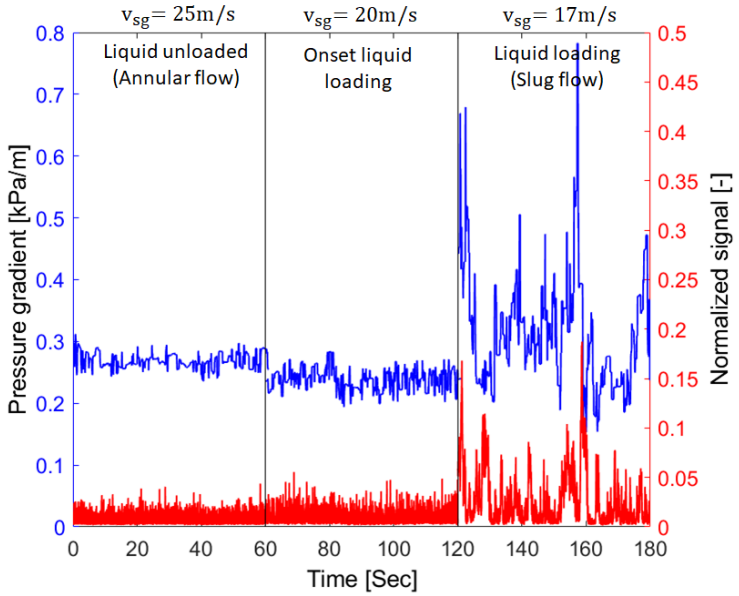

Fig. 2-2. Output signal of the differential pressure cell and conductance probe when reducing stepwise the gas rate (air-water system θ=30°, v_{sl}=0.01m/s)

Preliminary experiments were carried out to define a test matrix that could cover the annular-slug flow pattern transition. Limitations such as liquid volume in the tank, pump capacity and flow meter range meant that the test matrix had to be adjusted for different inclinations.

Superficial liquid from 0.01 to 0.2 m/s and gas velocities from 60 to 3 m/s were tested for water-air system inclination angles of 20° and 78° (Fig. 5-1). Data for air-water system inclination angles of 30°, 45°, 60° and 70° were collected by Vieira et al. (2019b). Data for the air-Exxsol D80 system was taken from Vieira et al. (2019a), as presented in Table 2-2.

Table 2-2 Experimental data for liquid loading air-water and air-Exxsol D80, 60mm ID at STP conditions. Vieira et al. (2019b) and Vieira et al. (2019a).

Pipe inclination (degree)	Air-water		Air-Exxsol D80	
	v_{sl} (m/s)	$v_{sg,omset\ LL}$ (m/s)	v_{sl} (m/s)	$v_{sg,omset\ LL}$ (m/s)
30	0.01	19.47	-	-
	0.02	22.4	0.02	18.49
	0.05	23.32	0.05	21.93
	0.1	21.78	0.1	22.43
	0.2	25.63	0.2	21.35
45	0.01	19.8	-	-
	0.02	21.46	0.02	21.96
	0.05	25.19	0.05	24.01
	0.1	24.76	0.1	24.3
	0.2	24.69	-	-
60	0.01	19.48	0.01	14.77
	0.02	21.72	-	-
	0.05	23.7	0.05	21.86
	0.1	25.57	0.1	24.29
	0.2	24.86	-	-
70	0.01	18.11	-	-
	0.02	20.03	-	-
	0.05	24.18	-	-
	0.1	23.47	-	-
	0.2	23.72	-	-

3. Proposed Model

The annular-slug transition boundary model proposed by Barnea (1986) is based on the assumption that the liquid film thickness distribution in the pipe cross section is constant for the whole range of pipe inclinations. It is also based on the assumption that the interfacial shear stress provided by the liquid phase that is required to maintain the annular flow structure of the dimensionless film thickness ($\tilde{\delta} = \delta/D$) for a given superficial liquid velocity v_{sL} is:

$$\tau_i = g(\rho_L - \rho_g)D \sin\beta\left(\widetilde{\delta_L} - \widetilde{\delta_L^2}\right)\left(1 - 2\widetilde{\delta_L}\right) + \frac{1}{32}C_L\rho_L\left(\frac{D\rho_l}{\mu_l}\right)^{-n}(v_{sL})^{2-n}\left[\frac{\left(1-2\widetilde{\delta_l}\right)}{\left(\widetilde{\delta_l} - \widetilde{\delta_l^2}\right)^2}\right] \quad 3\text{-}1$$

Shekhar et al. (2017) examined non-uniform film thickness distribution due to pipe inclination. They assumed that liquid loading would begin when the thicker film, at the bottom of the pipe, can no longer be carried by the gas phase. They therefore estimated the maximum film thickness that satisfied the required shear stress (using Equation 3-1) as ($\widetilde{\delta_{max}}$), and used an equation (Equation 1-8) to convert this into ($\widetilde{\delta_{avgL}}$). The corrected value was then used in Equation 3-1 to determine critical superficial gas velocity. The Shekhar et al. (2017) model therefore still uses the momentum equation from Barnea (1986), which was derived assuming an annular flow geometry for uniform liquid film thickness.

A different approach was used in this research work. The momentum balance equation for gas-liquid two-phase flow (Equation 3-2) is expressed in terms of the liquid holdup:

$$\tau_i S_i\left(\frac{1}{H_L} + \frac{1}{(1-H_L)}\right) - gA(\rho_l - \rho_g)\sin\theta - \tau_{wL}\frac{S_L}{H_L} = 0 \quad 3\text{-}2$$

Our model, similar to the work of Shekhar et al. (2017), still employs Equation 3-1 and the maximum liquid film thickness (δ_{maxL}). The real liquid area is, however, the main object of interest in the new model and is used to predict critical superficial gas velocity by employing Equation 3-2, which requires liquid holdup instead of liquid film thickness.

Expressions to correlate model variables versus holdup were derived using the data presented by Paz (1994), who experimentally investigated the effect of inclination angle on liquid film thickness distribution on a two-phase annular flow. A multi-probe was used to measure liquid film thickness at 0°, 45°, 90° and 180° around half the pipe, for inclination angles of 90°, 75°, 60° and 45° from the horizontal. Liquid superficial velocities ranging from 0.006 to 0.061 m/s and a gas superficial velocity of 18.29 m/s were used in this experiment.

The dimensionless liquid film thickness at several angular positions (φ) in the pipe cross section was computed from measured values taken from Paz (1994) and plotted against pipe inclination angle (θ) for different liquid superficial velocities. The data was fitted to an exponential function (Equation 3-3)

$$\widetilde{\delta_L}(\varphi, \theta) = a\, e^{-b\varphi} + c \quad 3\text{-}3$$

The function was integrated numerically in φ to obtain the area under the curve, which represents the cross-sectional area of liquid in the pipe from position 0º to 180º (shown in Fig. 5-2).

The liquid holdup was calculated from the cross-section area occupied by the liquid, as estimated above, and plotted against the maximum dimensionless liquid film thickness (at the bottom of the pipe), as shown in Fig. 3-1.

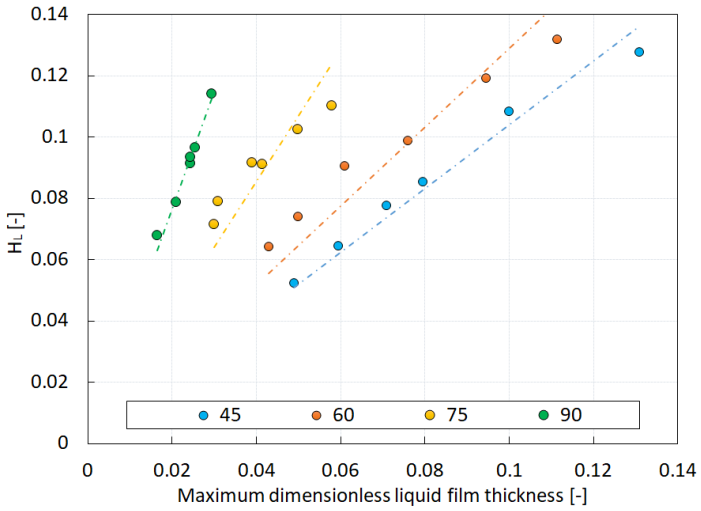

Fig. 3-1 Liquid holdup vs. maximum dimensionless liquid film thickness (measured at the bottom of the pipe)

There is a fairly linear relationship between these two variables. Liquid holdup can therefore be used to determine maximum film thickness, and can be described by a simple linear function of the single variable **a**.

$$H_L = a\widetilde{\delta_{maxL}} \qquad 3\text{-}4$$

The slope of the fitting lines (a) increases with increasing pipe inclination (θ). Both variables were plotted in Fig. 3-2.

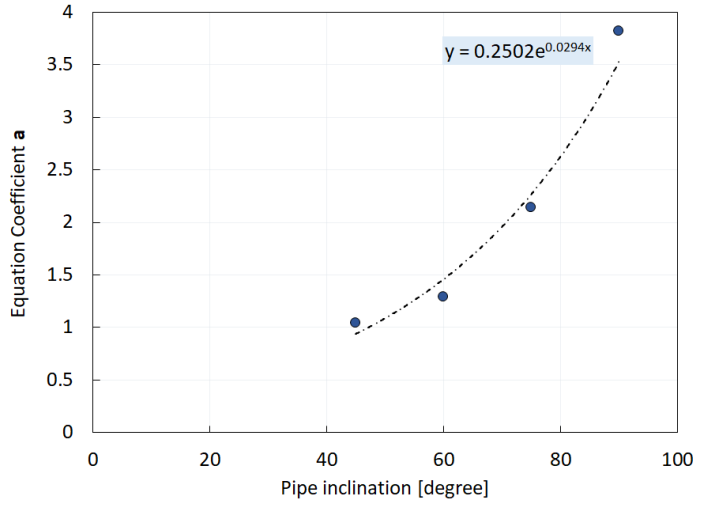

Fig. 3-2 Estimation of liquid holdup equation vs. pipe inclination (from horizontal)

The coefficient ***a*** can be seen to increase exponentially with increasing pipe inclination, their relationship being described by:

$$a = 0.25e^{0.0294\theta} \qquad 3\text{-}5$$

The change of liquid area (liquid holdup) due to pipe inclination also causes a change in the perimeter of the liquid-gas interface (S_i). The perimeter S_i was computed from Equation 3-3 from the functions created by fitting the Paz (1994) data, and plotted against liquid holdup (Fig. 3-3). Equation 3-6 is proposed to fit the data.

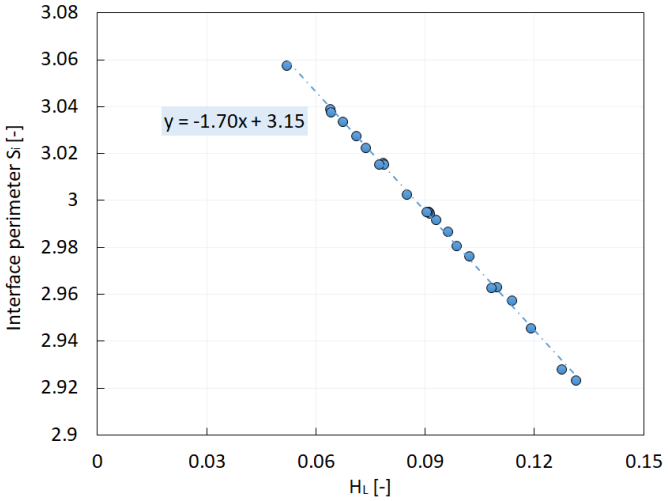

Fig. 3-3 Estimation of interface perimeter against liquid holdup

$$S_i = (\pi - 1.7H_L)D \tag{3-6}$$

The perimeter of the wall-liquid interface was calculated by $S_L = \pi D$. Wall shear stress was calculated by Equation 3-7, which was related to the local liquid velocity at the bottom of the pipe, and which is similar to that presented by Barnea (1986).

$$\tau_{wl} = \frac{1}{2} C_L \rho_l \left(\frac{\rho_l D v_{sL}}{\mu_L}\right)^{-n} \frac{v_{sL}^2}{4\left(\widetilde{\delta_{maxL}} - \widetilde{\delta_{maxL}}^2\right)} \tag{3-7}$$

where C_L and n are constants in the friction factor correlation, $C_L = 0.046$, $n = 0.2$ for turbulent liquid film and $C_L = 16$, $n = 1$ for laminar liquid film.

Substituting the relationship of S_L, S_i, H_L and the wall shear stress expression into Equation 3-2 and solving for interfacial shear stress yields

$$\tau_{i,liquid} = \frac{\tau_{wl}\frac{S_L}{H_L} + gA(\rho_l - \rho_g)\sin\theta}{S_i\left(\frac{1}{H_L} + \frac{1}{(1-H_L)}\right)} \tag{3-8}$$

The supplied interfacial shear stress provided by gas-phase was then estimated by Equation 3-9

$$\tau_{i,gas} = \frac{1}{2} f_l \frac{\rho_g v_{sg}^2}{\left(1 - 2\widetilde{\delta_{maxL}}\right)^4} \tag{3-9}$$

A new equation for calculating the interfacial friction factor based on the Paz (1994) data was also proposed. The steps leading up to the equation are explained in Appendix B section B-1.

$$f_i = f_g(98.87H_L + 2.2)\sin\theta \tag{3-10}$$

The superficial gas friction factor (f_g) was assumed to be 0.005 and the pipe inclination (θ) is expressed in radians.

Fig. 3-4 shows an overall flow chart for the annular-intermittent transition boundary (critical gas velocity) for an inclined pipe. Critical gas velocity is first determined from the input parameters, the momentum and continuity equations then being used to calculate the hydrodynamic behaviour of the two-phase flow.

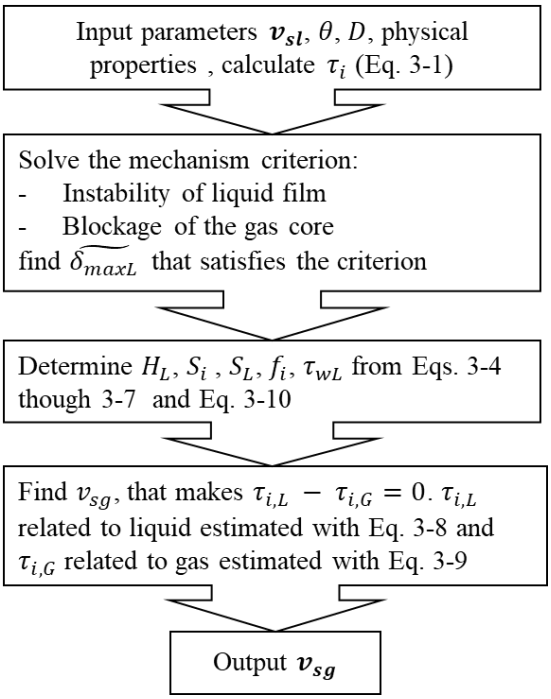

Fig. 3-4 Flow chart for calculating annular-slug flow transition boundary calculation

4. Model validation

We compared the results of the proposed model with both laboratory and field data, to confirm the new model's ability to predict the onset of liquid loading.

4.1 Laboratory data

Vieira et al. (2019a) and Vieira et al. (2019b) conducted experimental studies of liquid loading in an inclined 60 mm pipe. Vieira et al. (2019a) used inclinations of 30°, 45°, 60° and 70° for 0.01, 0.02, 0.05, 0.1 and 0.2 m/s of v_{sL}, water being the liquid phase of a two-phase gas-liquid system. Vieira et al. (2019b) used pipe inclinations of 45°, 60° and 70° for 0.01, 0.02, 0.05, 0.1 and 0.2 m/s of v_{sL}, light oil (Exxsol D80) being the liquid phase. Both experiments yielded to a critical gas velocity ($v_{sg,omset\ LL}$) for every v_{sL}.

Transition boundaries were calculated and plotted using the experimental data and the new model for liquid loading prediction. Predictions from the Barnea (1986) and Shekhar et al. (2017) models were also plotted for comparison.

Discrete experimental points from the air-water system were plotted on a logarithmic scale (Fig. 4-1a – Fig. 4-1f), the continuous-line representing the annular-slug transition boundary for the new model. Transitions estimated using the Barnea (1986) and Shekhar et al. (2017) models are plotted as dashed-lines. An error bar was added to the data points (onset LL) to show the variability of the measured critical gas velocity, the right length of the horizontal error bar representing the last full stable production (annular flow) and the left length the first full unstable production (slug flow). The two flow patterns were identified by visual inspection.

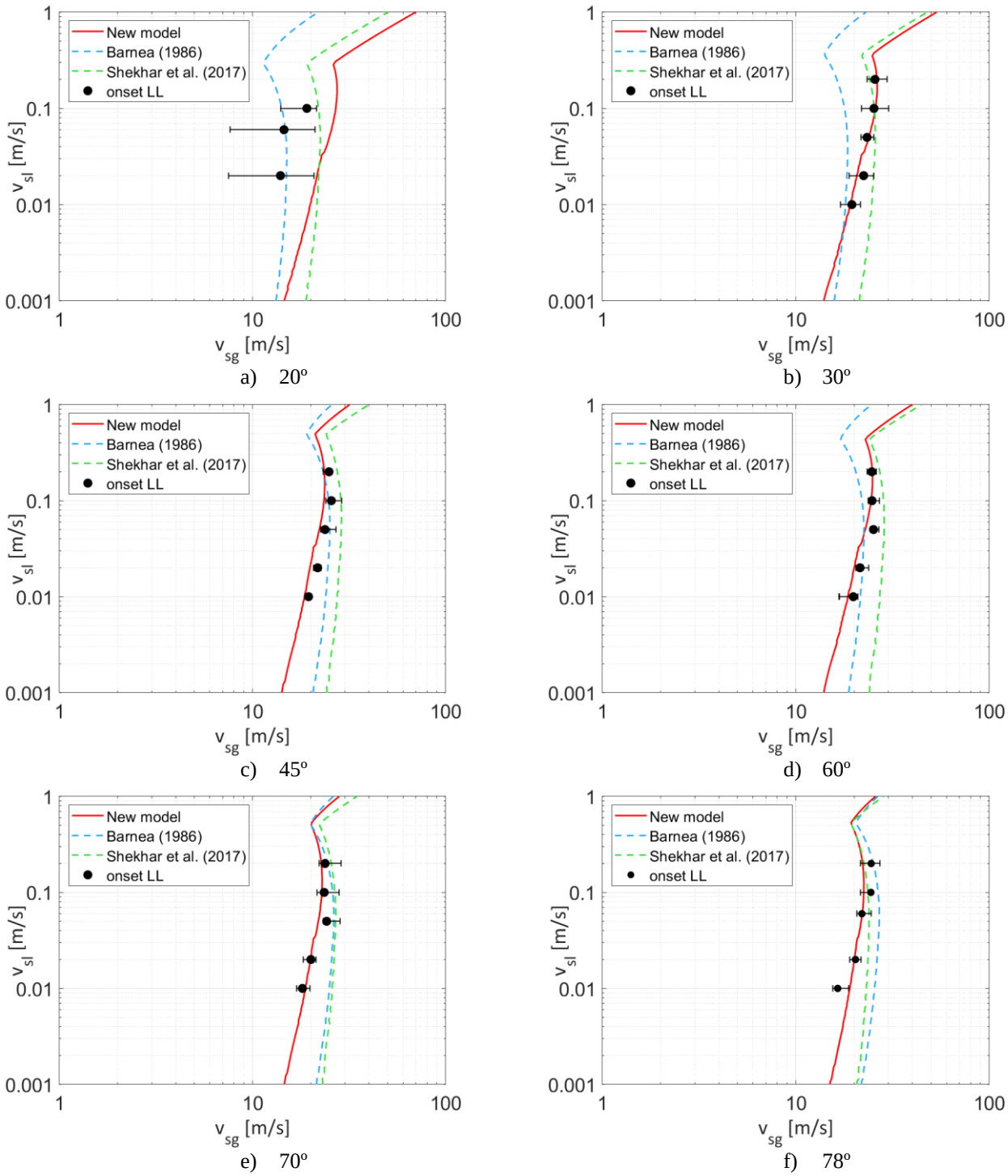

a) 20º b) 30º

c) 45º d) 60º

e) 70º f) 78º

Fig. 4-1 Comparison between Vieira et al. (2019b) and collected experimental data with transition boundary prediction by the new model, the model by Barnea (1986) and the model by Shekhar et al. (2017), for air-water system at STP condition

Fig. 4-2a – Fig. 4-2c presents the same analysis, but with air-Exxsol D80 discrete data point.

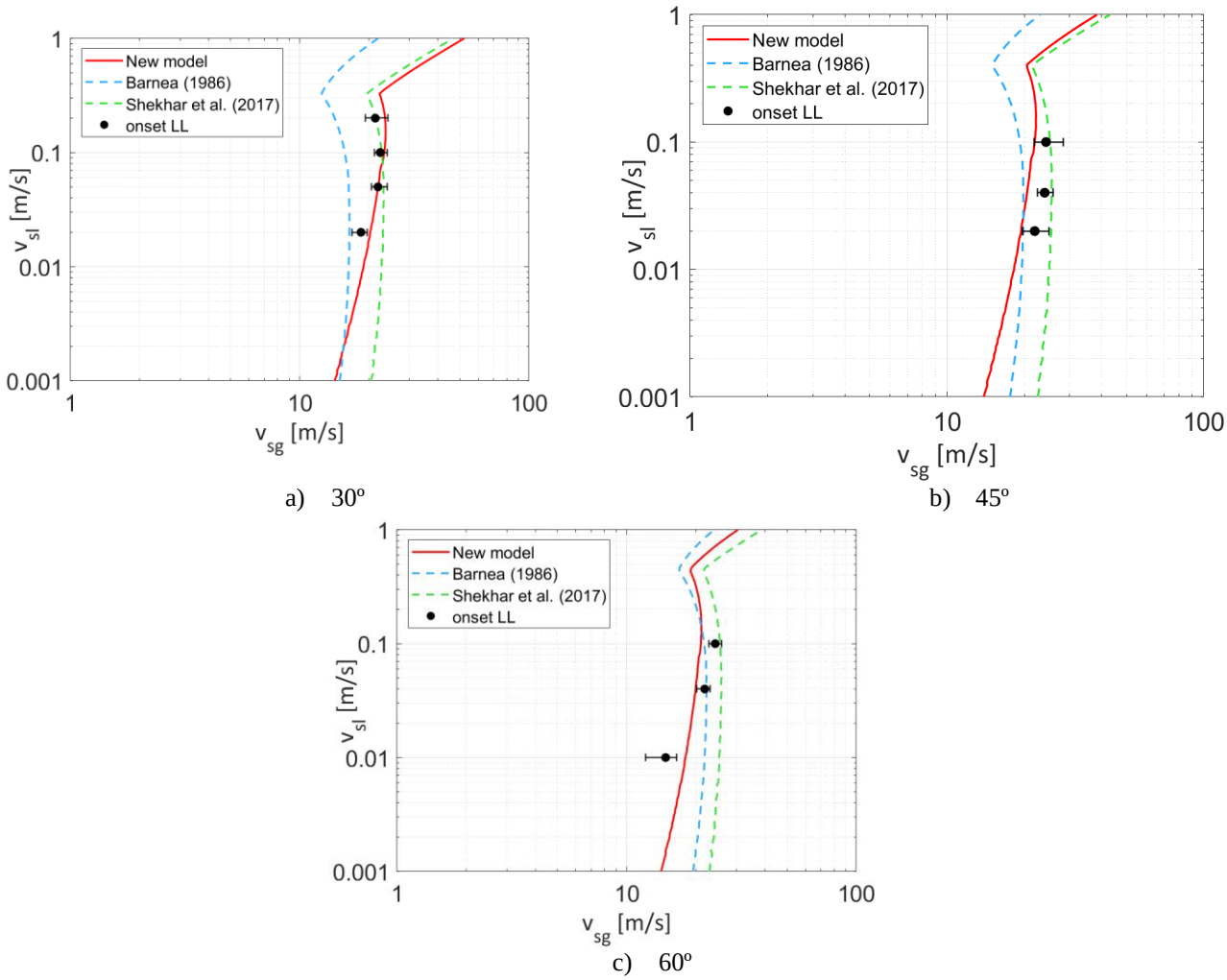

a) 30º b) 45º

c) 60º

Fig. 4-2 Comparison between experimental data by Vieira et al. (2019a) and the transition boundary prediction by the new model, the model by Barnea (1986) and the model by Shekhar et al. (2017), for air-Exxsol D80 system at STP condition

Agreement between predictions of the new model and experimental measurements is fairly good, in most cases. This can indicate that the model is generic and can be extrapolated to other operational conditions than those from which it was derived (experimental data of Paz (1994)). The model performs, however, poorly for the lowest inclination in air-water flow (Fig. 4-1a). This could be because the data of Paz (1994) does not include inclinations below 45º.

Fig. 4-1b and Fig. 4-2a show that the model agreed with the experimental measurements, even though pipe inclination is below 45º. This could be due to the fact that the conditions at 30º inclination are not significantly different to those at 45º. The difference might, however, be significant for an inclination of 20º, as the liquid film might not reach the top of the pipe.

Fig. 4-3 shows the comparison of every individual observed critical gas velocity predicted by the present model and the measured data.

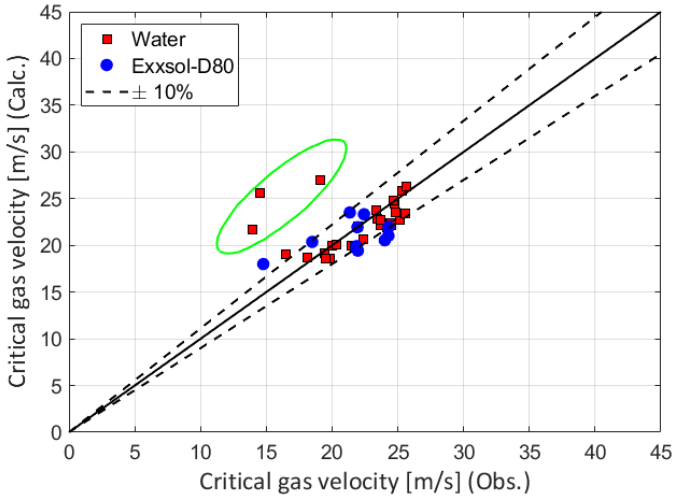

Fig. 4-3 Comparison between Vieira et al. (2019a), Vieira et al. (2019b) and collected experimental data vs. values predicted by the new model

The 45º-line in the Fig. 4-3 plot represents the annular-slug transition boundary. It can be seen that predicted critical gas velocities lay close to the line, variation being approximately 10%. It was also noted that the model overestimates critical gas velocity values at a pipe inclination of 20º (points in the green ellipse).

Computations were further treated statistically, to validate and quantify the accuracy of the model. Experimental and calculated data were compared point by point. For each data point, a relative error was determined by:

$$Err_{abs,X} = \left| \frac{X_{calculated} - X_{measured}}{X_{measured}} \right| \quad 4\text{-}1$$

where X stands for a physical variable critical gas velocity, $X_{calculated}$ is the model prediction value and $X_{measured}$ is the experimental (measured) value.

Then an average percent error was determined by

$$Err_{avg,X} = \frac{100}{n} \sum_{1}^{n} Err_{abs,X} \quad 4\text{-}2$$

n being the number of data points in the data set.

Table 4-1 presents the average error calculated for each pipe inclination for all the data points for the air-water and air-Exxsol D80 systems.

Table 4-1. Average error for the air-water and air-Exxsol D80 systems.

	Air-water			Air-Exxsol D80		
Pipe inclination [º]	New model E_{avg}[%]	Shekhar et al. (2017) E_{avg}[%]	Barnea (1986) E_{avg}[%]	New model E_{avg}[%]	Shekhar et al. (2017) E_{avg}[%]	Barnea (1986) E_{avg}[%]
20	57.50	42.54	11.66	-		
30	3.22	11.11	22.49	6.10	8.09	24.98
45	4.91	20.88	10.25	11.85	8.77	16.00
60	6.68	23.13	10.43	14.73	31.24	19.86
70	4.14	21.40	17.69	-		
78	7.01	15.42	23.79	-		
All data	10.8	20.9	16.9	10	15.2	20.8

Comparing the results for the air-water system shows improvement, the new model achieving an average error of 10.8% for the prediction of critical gas velocity for all inclinations, as opposed to 20.9% for Shekhar et al. (2017) and 16.9% for Barnea (1986). A similar trend was observed for air-Exxsol D80. The new model shows a lower error of 10% as opposed to 15.2% for Shekhar et al. (2017) and 20.8% for Barnea (1986).

Experimental data publish by Guner (2012) for a two-phase air-water system was used to further evaluate the performance of the new proposed model. He performed experiments in a 3-inch ID pipe at inclination angles of 90º, 75º, 60º and 45º from the horizontal, using superficial liquid velocities of 0.01, 0.05 and 0.1 m/s and superficial gas velocities ranging from approximately 40-2m/s.

The set of discrete data points defined by Guner (2012) as the onset of film reversal, complete film reversal (critical v_{sg}) and no loading were used. The complete film reversal data points were used as the left length of the horizontal error bars, the no loading being the right length for the first full unstable production.

Fig. 4-4 shows the comparison of the discrete data with the prediction from the new model, Barnea (1986) and Shekhar et al. (2017).

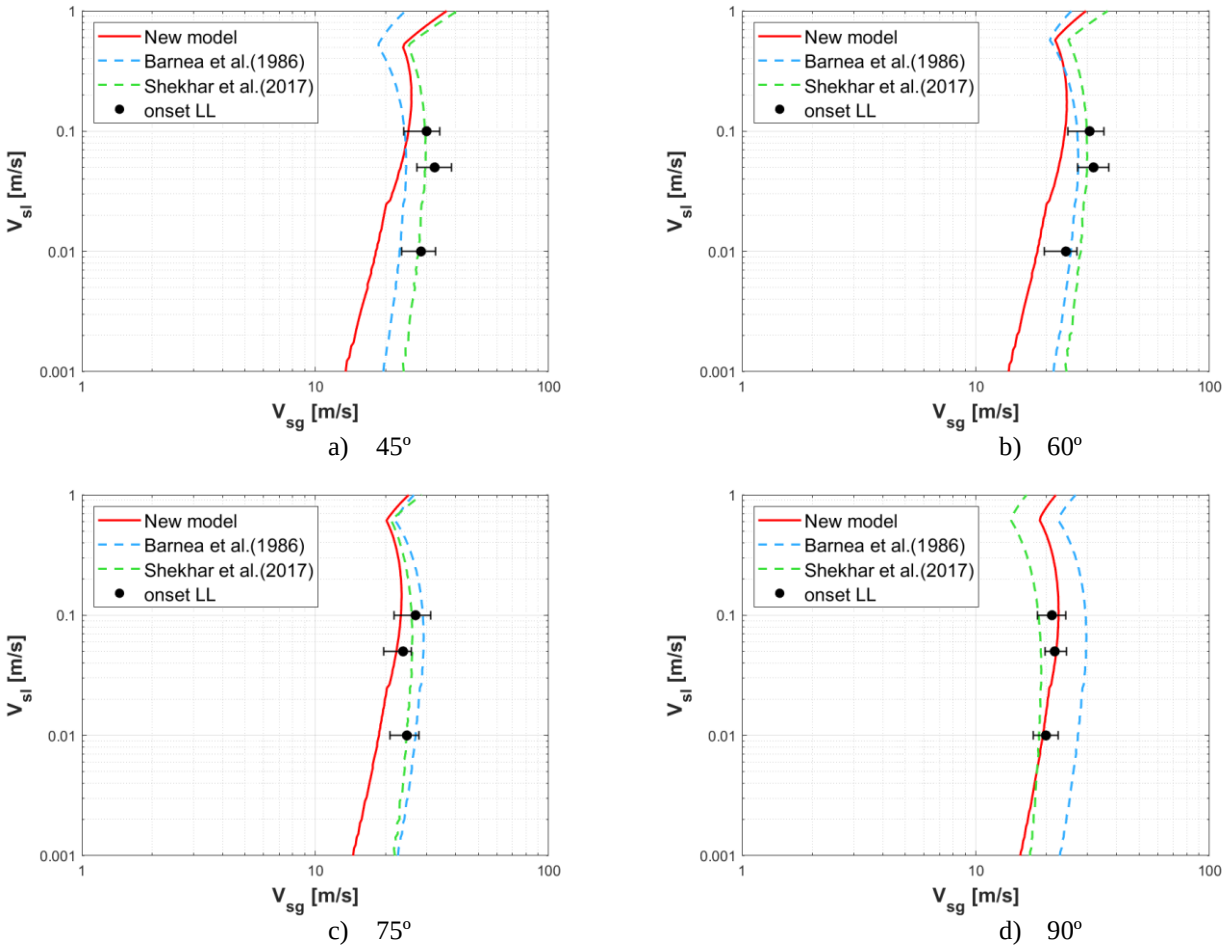

a) 45º b) 60º

c) 75º d) 90º

Fig. 4-4 Comparison between Guner (2012) experimental data and the transition boundary prediction by the new method, Barnea (1986) and Shekhar et al. (2017)

The overall agreement between the new model prediction and Guner (2012) experimental data is fairly good in most cases. The new model, however, predicted poorly compared to the Shekhar et al. (2017) model, giving a more than 25% error (Fig. 4-5).

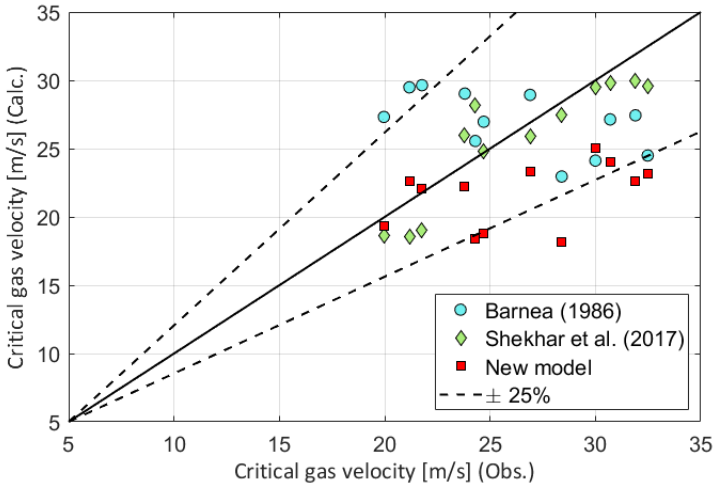

Fig. 4-5 Comparison between Guner (2012) experimental data vs. predicted values by the new method, Barnea (1986) and Shekhar et al. (2017)

It is worthwhile mentioning that the this data was also published by Guner et al. (2015). Critical superficial gas velocity values are the same as those published previously as loaded conditions past the onset point. The author of this paper has, however, assumed that the published values are velocities for the liquid loading onset. The results will therefore vary if this is not correct.

4.2 Field data

Three different sets of field data were used to evaluate the performance of the new method in predicting liquid loading onset.

Analysis of the field data revealed accurate prediction required the upwards adjustment of approximately 0.4 of the interfacial friction factor, for cases of low liquid holdup. A coefficient was therefore added to Equation 3-10, Equation 4-3 therefore being

$$f_i = 0.4 f_g (98.87 H_L + 2.2) \sin\theta \qquad H_L < 0.05 \tag{4-3}$$

The prediction accuracy for the datasets described in section 4.1 deteriorated, when this modification was introduced, by 10% to 50% relative error. Model prediction is, however, conservative (i.e. lower predicted critical gas velocities). Fig. 4-6 shows the comparison between measured and predicted data for the dataset presented by Vieira et al. (2019a) and Vieira et al. (2019b). A similar behaviour was observed for the Guner (2012) experimental data (Fig. 4-7).

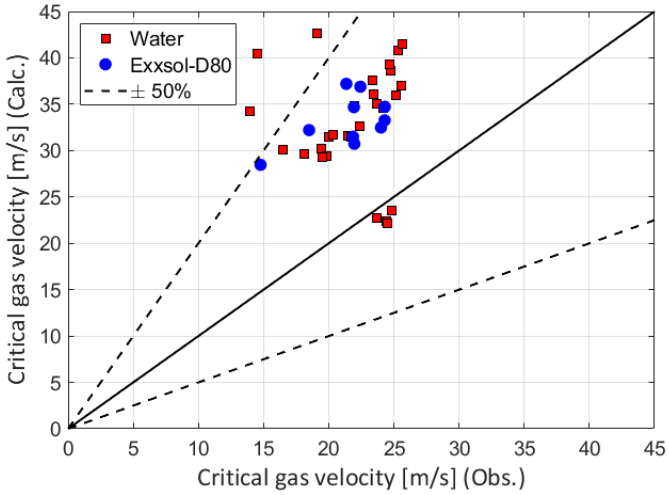

Fig. 4-6 Comparison between Vieira et al. (2019a), Vieira et al. (2019b) and gathered experimental data vs. values predicted by the new model with adjustment factor

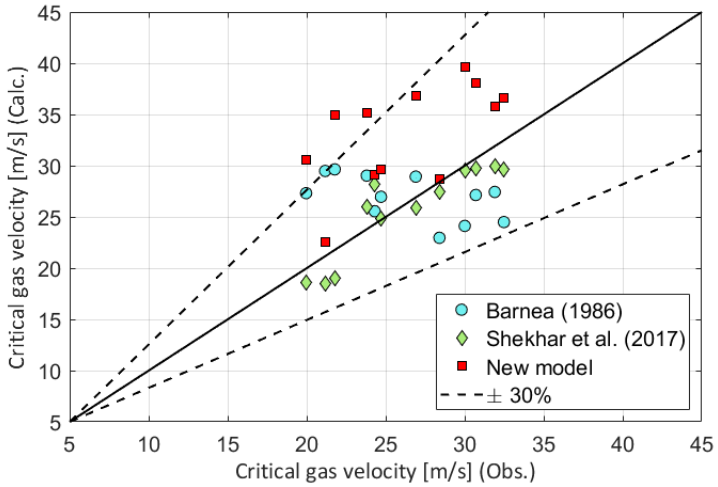

Fig. 4-7 Comparison between Guner (2012) experimental data vs. values predicted by the new model with adjustment factor

Measured field data was plotted in a 45°-line plot and compared with the new model prediction and the other studied models. This is shown in Fig. 4-8 to Fig. 4-11. The 45°-line in the plot represents the loaded and unloaded transition boundary. An ideal model will therefore show field data that is reported as being the onset of liquid loading slightly above the line and the average error as low as possible. This indicates that the model is predicting the field data with a high degree of accuracy.

The first field data used in the study was published by Veeken et al. (2010) for 67 North Sea gas wells that were starting to experience liquid loading. The gas wells had tubing diameters of 2–6 inches and included vertical and inclined pipe geometries (0° to 64° inclination angles from vertical). Condensate and water were produced, the liquid gas ratio being assumed to be 5 bbl/MMcf in the calculation as recommended by Luo et al. (2014). The test gas rate reported in their paper was converted to superficial gas velocity.

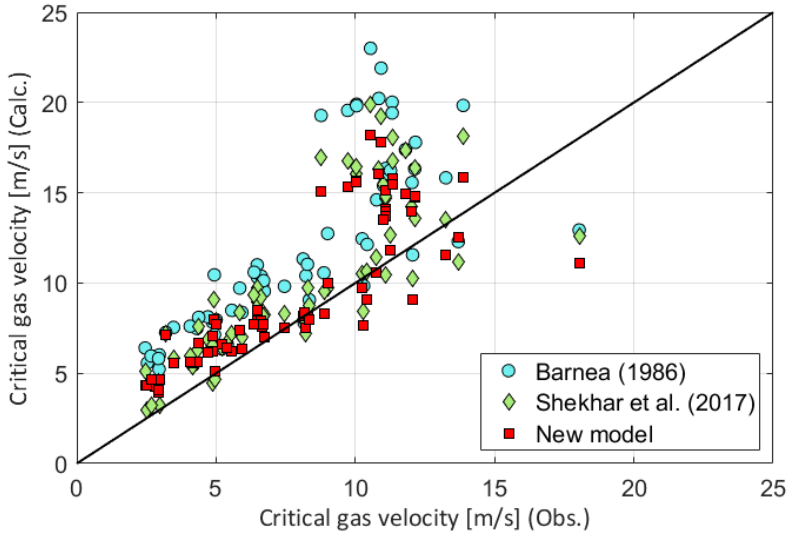

Fig. 4-8 Comparison between Veeken et al. (2010) data vs. values predicted by the new model

Table 4-2 Critical gas velocities prediction for Veeken et al. (2010) data

Model	Well correctly predicted	E_{avg}[%]
Barnea (1986)	62/67	59.07
Shekhar et al. (2017)	57/67	35.73
New model	55/67	31.17

It is clear from the results in Table 4-2 that the new models exhibit greater accuracy than the other models. The number

of wells predicted correctly is, however, almost the same.

The second field data used in model evaluation was published by Belfroid et al. (2008) for two gas wells. Both wells used an inclined pipe geometry of 40° (from vertical). One well had a tubing diameter of 0.112 m and observed critical gas rate of 90 000 Sm^3/d, the other a tubing diameter of 0.074 m and critical gas rate of 45 000 Sm^3/d. Calculations were performed using the data given in their publications. The wells were reported as being in the critical condition. The predicted results were expected to be above the 45°-line, as seen in Fig. 4-9

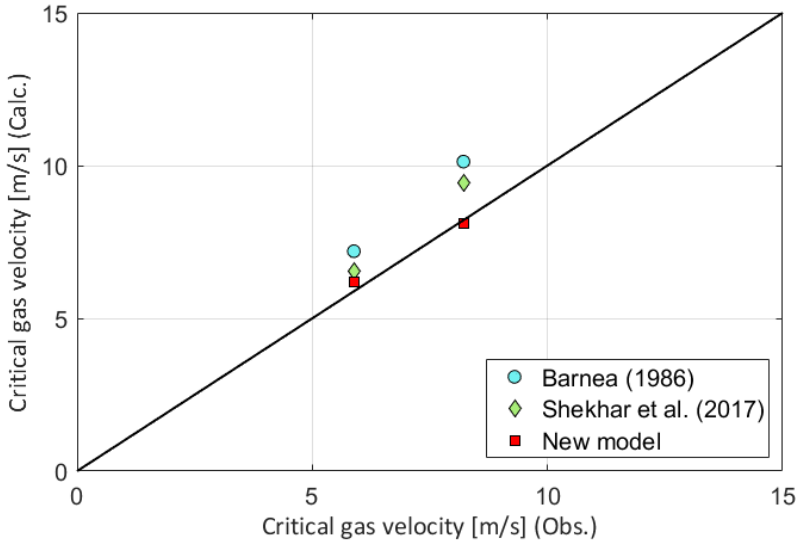

Fig. 4-9 Comparison between Belfroid et al. (2008) data vs. values predicted by the new model

Table. 4-3 Critical gas velocities prediction for Belfroid et al. (2008) data

Model	Well correctly predicted	E_{avg}[%]
Barnea (1986)	2/2	22.82
Shekhar et al. (2017)	2/2	12.91
New model	2/2	1.98

Table. 4-3 shows that the new model gives a better critical gas velocity prediction, as shown by a lower average error than the other methods, which corresponds to the Veeken et al. (2010) data

The third field data set used to evaluate the model is the well production data published by Turner et al. (1969), which is field data for 90 gas wells, 37 experiencing liquid loading and 53 producing at stable conditions. This means that there was no liquid accumulation in the wellbore (unloaded), and all the wells were vertical (0° inclination angle). The gas rates tested and reported by Turner were converted to superficial gas velocities, which were then used to compare with the critical gas velocities from the new model. The comparison was performed for every well, as shown in Fig. 4-10 and Fig. 4-11.

The well was considered to be loaded when the calculated velocity was higher than the observed, and unloaded where the calculated critical gas velocity was lower than the observed. The well data for unloaded wells was slightly below the 45°-line on the plot.

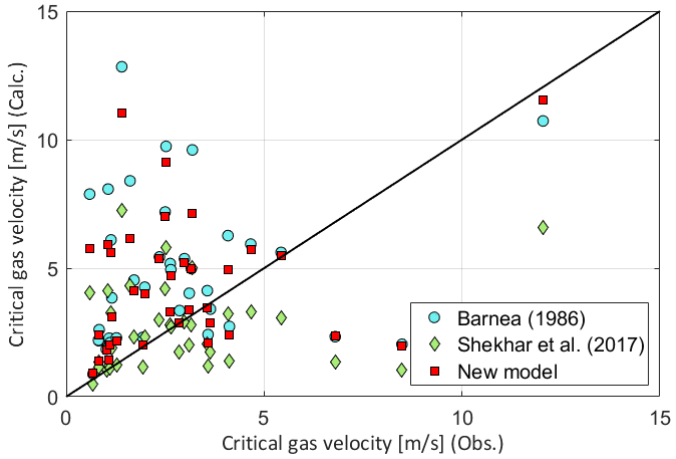

Fig. 4-10 Comparison between Turner et al. (1969) data (loaded) vs. values predicted by the new model

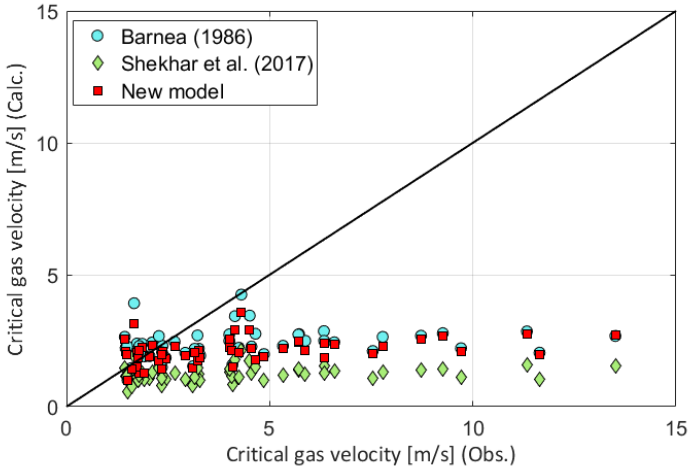

Fig. 4-11 Comparison between Turner et al. (1969) data (unloaded) vs. values predicted by the new model

Tab. 4-4 Critical gas velocities prediction for Turner et al. (1969) (loaded) data

Model	Well correctly predicted	E_{avg}[%]
Barnea (1986)	31/37	176.72
Shekhar et al. (2017)	20/37	78.09
New model	29/37	134.44

Tab. 4-5 Critical gas velocities prediction for Turner et al. (1969) (unloaded) data

Model	Well correctly predicted	E_{avg}[%]
Barnea (1986)	41/53	42.04
Shekhar et al. (2017)	51/53	60.64
New model	44/53	44.43

The prediction of unloaded wells was conservative for all models i.e. well data was below the 45°-line. The new model did not, however, exhibit a significantly better accuracy than the observed data. The new model is shown to be conservative, as almost all wells are correctly predicted with a considerable degree of accuracy. The loaded data reported by Turner et al. (1969), which is measured after the onset of liquid loading, differs from the other field data evaluated. This means that an ideal approach for this data is defined by the number of wells correct predicted.

The new model that is proposed performed overall better on our experimental data than the Barnea (1986) and Shekhar et al. (2017) models. Performance was also better for the field data, which represents an improvement.

The suggested model performed well. It is, however, recommended that further and future work investigates methods for verifying the applicability of the equations that have been developed (and improve them if necessary) using experimental data for other pipe diameters, test fluids and extended liquid holdup ranges.

5. Conclusion

This work presents a new model for estimating liquid loading onset in inclined pipes based on film reversal and on flow pattern transition from annular to intermittent flow. Auxiliary model correlations were developed using experimental data published by Paz (1994).

1. The distinctive features of the new model are:
    a) The momentum balance equation for annular flow is expressed as a function of liquid holdup instead of liquid thickness. The effect of the non-uniform film distribution in the pipe cross-section is therefore captured by the variation in liquid holdup.
    b) A new interfacial friction factor equation was developed as a function of liquid holdup.
    c) This model should be restricted to upward pipe inclinations (30° to 90° from horizontal), liquid viscosities of 1.1cP and 0.018 cP, superficial gas velocities of 3-60 m/s and liquid velocities of 0.01-0.2m/s. Results show that the model performs poorly when applied to pipe inclinations lower than 30° from the horizontal.
2. The model provided accurate predictions of critical gas velocities for the experimental data collected by the author for water-air and oil-air in inclined pipes. The model showed a better accuracy than the predictions provided by the two existing models.
3. The model provided conservative predictions of critical gas velocities of previously published experimental data for water-air and oil-air in inclined pipes. It showed a better accuracy than the two existing models.
4. An upwards adjustment of the interface friction factor was required to improve model accuracy and reproduce the field data reported in previous work.

Nomenclature

A	Pipe cross-section area (m^2)
A_G	Cross-section gas core area (m)
A_L	Cross-section liquid area (m)
D	Pipe diameter (m)
f_i	Interfacial friction factor (-)
f_{WL}	Liquid-wall friction factor (-)
g	Gravity acceleration (m/s^2)
H_L	Liquid holdup (-)
p	Pressure (Pa)
v_{sg}	Superficial gas velocity (m/s)
v_{sL}	Superficial liquid velocity (m/s)
Re	Reynolds number (-)
S_i	Interfacial perimeter (m)
S_L	Wetted perimeter (m)
	Greek Symbols
δ_L	Liquid film thickness (m)
ρ_G	Gas core density (kg/m^3)
ρ_L	Liquid core density (kg/m^3)
σ	Gas-liquid interfacial tension (N/m)
τ_i	interfacial shear stress (Pa)
τ_{wL}	Wall shear stress (Pa)
μ_G	Gas viscosity (cP)
μ_L	Liquid viscosity (cP)
θ	Pipe inclination from horizontal (degree)

Acknowledgments

The authors would like to thank the Department of Geoscience and Petroleum (IGP) and the Department of Energy and Process Engineering (EPT) at the Norwegian University of Science and Technology (NTNU) and its staff for their support of this research.

REFERENCES

ALSAADI, Y. 2013. *Liquid Loading in Highly Deviated Gas Wells.* Msc degree, University of Tulsa.

BARNEA, D. 1986. Transition from annular flow and from dispersed bubble flow—unified models for the whole range of pipe inclinations. *International journal of multiphase flow,* 12**,** 733-744.

BARNEA, D. 1987. A unified model for predicting flow-pattern transitions for the whole range of pipe inclinations. *International Journal of Multiphase Flow,* 13**,** 1-12.

BELFROID, S., SCHIFERLI, W., ALBERTS, G., VEEKEN, C. A. & BIEZEN, E. Predicting onset and dynamic behaviour of liquid loading gas wells. SPE Annual Technical Conference and Exhibition, 2008. Society of Petroleum Engineers.

CHUPIN, G., HU, B., HAUGSET, T., SAGEN, J. & CLAUDEL, M. Integrated wellbore/reservoir model predicts flow transients in liquid-loaded gas wells. SPE Annual Technical Conference and Exhibition, 2007. Society of Petroleum Engineers.

COLEMAN, S. B., CLAY, H. B., MCCURDY, D. G. & NORRIS III, L. H. 1991. A new look at predicting gas-well load-up. *Journal of Petroleum Technology,* 43**,** 329-333.

DUGGAN, J. O. 1961. Estimating Flow Rates Required To Keep Gas Wells Unloaded.

FERNANDEZ, J. J., FALCONE, G. & TEODORIU, C. 2010. Design of a high-pressure research flow loop for the experimental investigation of liquid loading in gas wells. *SPE Projects, Facilities & Construction,* 5**,** 76-88.

FIEDLER, S. & AURACHER, H. 2004. Experimental and theoretical investigation of reflux condensation in an inclined small diameter tube. *International journal of heat and mass transfer,* 47**,** 4031-4043.

FLORES-AVILA, F. S., SMITH, J. R., BOURGOYNE JR, A. T. & BOURGOYNE, D. A. Experimental evaluation of control fluid fallback during off-bottom well control: effect of deviation angle. IADC/SPE Drilling Conference, 2002. Society of Petroleum Engineers.

FORE, L., BEUS, S. & BAUER, R. 2000. Interfacial friction in gas–liquid annular flow: analogies to full and transition roughness. *International journal of multiphase flow,* 26**,** 1755-1769.

GUNER, M. 2012. *Liquid Loading of gas wells with deviation from 0º to 45º.* Master of science, University of Tulsa.

GUNER, M., PEREYRA, E., SARICA, C. & TORRES, C. An experimental study of low liquid loading in inclined pipes from 90° to 45°. SPE production and operations symposium, 2015. Society of Petroleum Engineers.

GUO, B., GHALAMBOR, A. & XU, C. A systematic approach to predicting liquid loading in gas wells. SPE Production Operations Symposium, 2005. Society of Petroleum Engineers.

JONES, P. J. 1946. *Petroleum Production: The optimum rate of production*, Reinhold Publishing Corporation.

KELKAR, M. G., PEREYRA, E. J., SKOPICH, A. & SARICA, C. Pipe Diameter Effect on Liquid Loading in Vertical Gas Wells. SPE Production and Operations Symposium, 2013. Society of Petroleum Engineers.

LI, M., LEI, S. & LI, S. 2001. New View on Continuous-removal Liquids from Gas Wells. *SPE Permian Basin Oil and Gas Recovery Conference.* Midland, Texas: Society of Petroleum Engineers.

LUO, S., KELKAR, M., PEREYRA, E. & SARICA, C. 2014. A new comprehensive model for predicting liquid loading in gas wells. *SPE Production & Operations,* 29**,** 337-349.

NOSSEIR, M., DARWICH, T., SAYYOUH, M. & EL SALLALY, M. A new approach for accurate prediction of loading in gas wells under different flowing conditions. SPE Production Operations Symposium, 1997. Society of Petroleum Engineers.

PAZ, R. J. 1994. Film Thickness Distribution for Annular Flow in Directional Wells: Horizontal to Vertical. *SPE Annual Technical Conference and Exhibition.* New Orleans, Louisiana: Society of Petroleum Engineers.

SARICA, C., YUAN, G., SUTTON, R. P. & PEREYRA, E. J. An experimental study on liquid loading of vertical and deviated gas wells. SPE Production and Operations Symposium, 2013. Society of Petroleum Engineers.

SHEKHAR, S., KELKAR, M., HEARN, W. J. & HAIN, L. L. 2017. Improved Prediction of Liquid Loading In Gas Wells. *SPE Production & Operations*.

SHOHAM, O. 2006. *Mechanistic modeling of gas-liquid two-phase flow in pipes,* Richardson, Tex Society of Petroleum Engineers

SUTTON, R. P., COX, S. A., LEA, J. F. & ROWLAN, O. L. 2010. Guidelines for the proper application of critical velocity calculations. *SPE Production & Operations,* 25**,** 182-194.

TAITEL, Y. & DUKLER, A. 1976. A model for predicting flow regime transitions in horizontal and near horizontal gas- liquid flow. *AIChE Journal,* 22**,** 47-55.

TURNER, R., HUBBARD, M. & DUKLER, A. 1969. Analysis and prediction of minimum flow rate for the continuous removal of liquids from gas wells. *Journal of Petroleum Technology,* 21**,** 1,475-1,482.

VAN 'T WESTENDE, J. M. C., KEMP, H. K., BELT, R. J., PORTELA, L. M., MUDDE, R. F. & OLIEMANS, R. V. A. 2007. On the role of droplets in cocurrent annular and churn-annular pipe flow. *International Journal of Multiphase Flow,* 33**,** 595-615.

VEEKEN, K., HU, B. & SCHIFERLI, W. 2010. Gas-well liquid-loading-field-data analysis and multiphase-flow modeling. *SPE Production & Operations,* 25**,** 275-284.

VIEIRA, C. & STANKO, M. Applicability of Models for Liquid Loading Prediction in Gas Wells. SPE Europec featured at

81st EAGE Conference and Exhibition, 2019a. Society of Petroleum Engineers.
VIEIRA, C. & STANKO, M. Effect of droplet entrainment in liquid loading prediction. BHR 19th International Conference on Multiphase Production Technology, 2019b. BHR Group.
VITTER, A. L., JR. 1942. Back-Pressure Tests On Gas-Condensate Wells. *Drilling and Production Practice*. New York, New York: American Petroleum Institute.
WALLIS, G. B. 1969. *One-dimensional two-phase flow*, New York, McGraw-Hill.
WALTRICH, P. J., POSADA, C., MARTINEZ, J., FALCONE, G. & BARBOSA JR, J. R. 2015. Experimental investigation on the prediction of liquid loading initiation in gas wells using a long vertical tube. *Journal of Natural Gas Science and Engineering*, 26**,** 1515-1529.
WANG, Y.-W., ZHANG, S.-C., YAN, J. & CHEN, W.-B. 2010. A new calculation method for gas-well liquid loading capacity. *Journal of Hydrodynamics, Ser. B,* 22**,** 823-826.
WANG, Z., GUO, L., WU, W., ZHU, S. & ZHOU, H. 2016. Experimental study on the critical gas velocity of liquid-loading onset in an inclined coiled tube. *Journal of Natural Gas Science and Engineering*, 34**,** 22-33.
ZABARAS, G., DUKLER, A. & MOALEM- MARON, D. 1986. Vertical upward cocurrent gas- liquid annular flow. *AIChE journal*, 32**,** 829-843.

Appendix A Experimental results

The data collected from the experiments performed in this work are presented below:

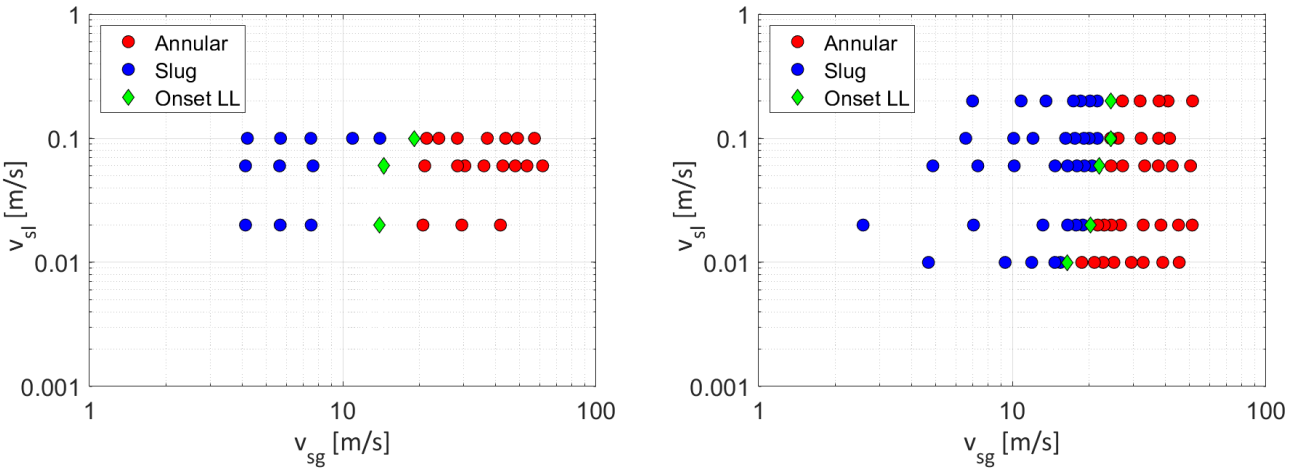

20º 78º

Fig. 5-1. Experimental tests on transition boundary of annular-slug for air-water at STP condition for different inclination angles (from horizontal)

Appendix B New Model

Paz (1994) performed an experimental investigation of two-phase annular flow and the effect of inclination angle on the liquid film thickness distribution around the circumferential of the pipe. Fig. 5-2 shows the fitting of the Paz (1994) data for the estimation of liquid area.

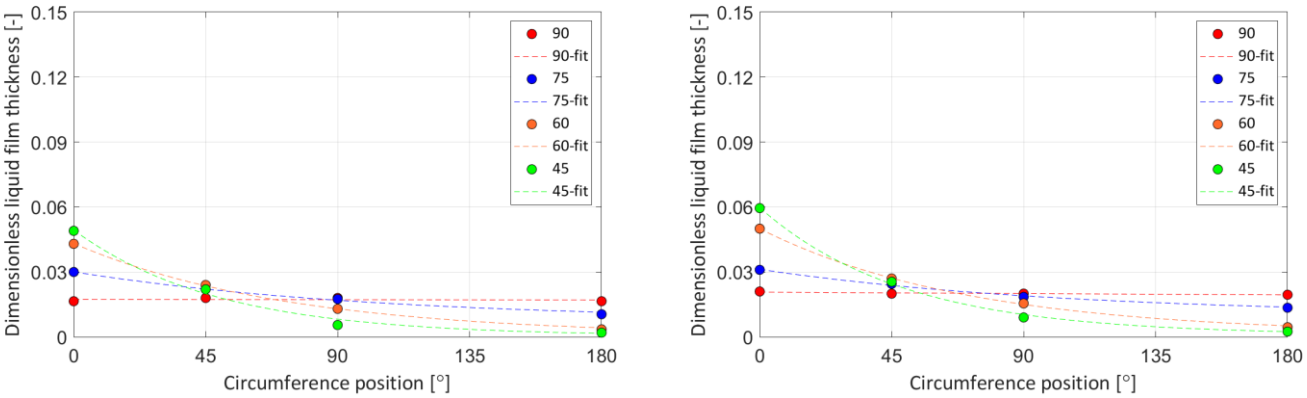

a) $v_{sl} = 0.006\, m/s$ b) $v_{sl} = 0.012\, m/s$

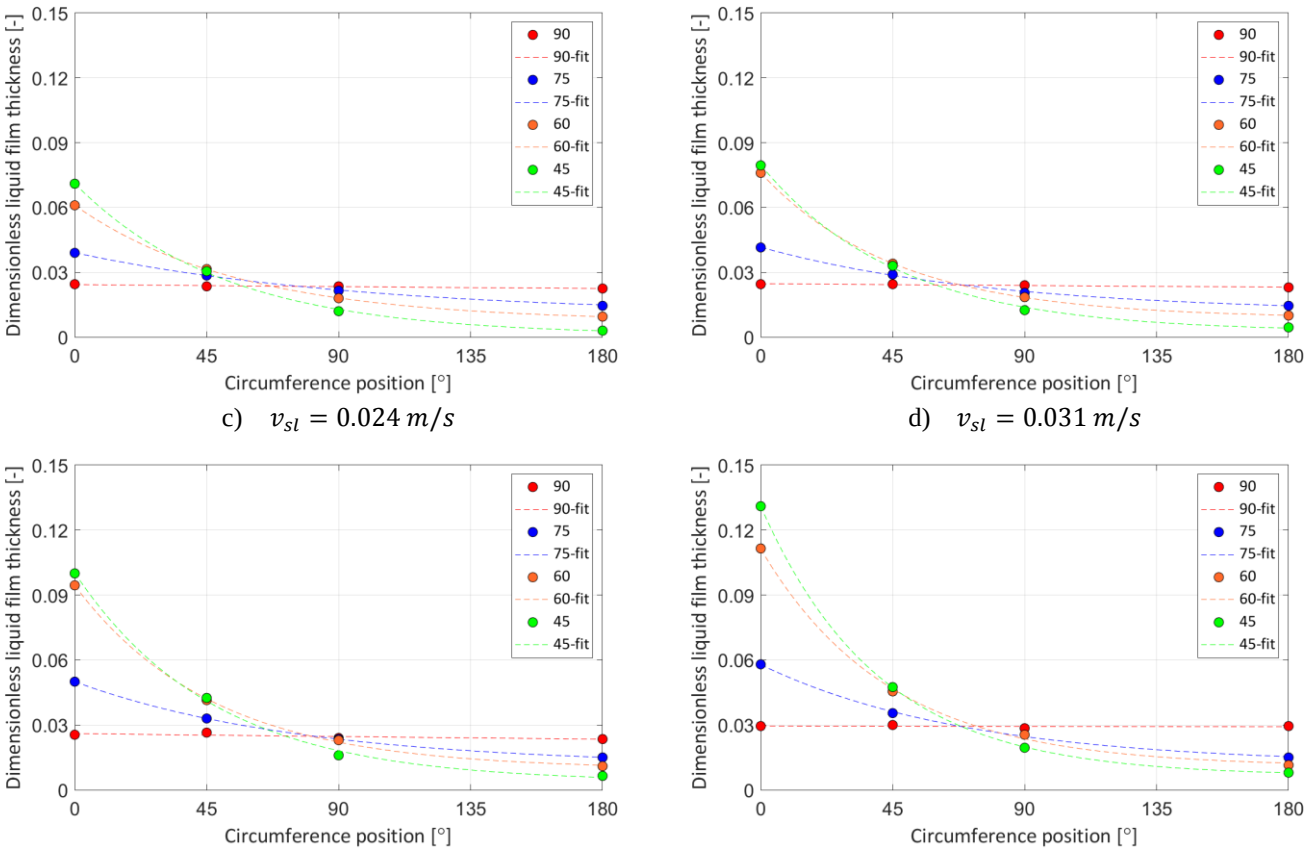

c) $v_{sl} = 0.024\ m/s$ d) $v_{sl} = 0.031\ m/s$

e) $v_{sl} = 0.046\ m/s$ $v_{sl} = 0.061\ m/s$

Fig. 5-2 Fitting Paz (1994) data at $v_{sg} = 18.29\ m/s$

B-1 Interfacial friction factor - new equation

The steps involved in the development of the proposed interface friction factor equation using the experimental data of Paz (1994) are presented below:

1. Calculate the liquid friction factor

$$f_L = C_L \left(\frac{\rho_L v_L^2}{\mu_L} \right)^{-n} \tag{5-1}$$

where $D_L = 4A_L/L$ is the hydraulic diameter, μ_L is the liquid viscosity and C_L and n are constants in the friction factor correlation, $C_L = 0.046$, $n = 0.2$ for turbulent liquid film and $C_L = 16$, $n = 1$ for laminar liquid film, the respective liquid velocity being

$$v_L = \frac{v_{sL} A}{A_L} \tag{5-2}$$

2. Calculate the liquid cross section area by multiplying liquid holdup (Fig. 3-1) with pipe area.
3. Calculate liquid shear stress (τ_{wL}) using Equation 5-3, actual liquid velocity being estimated using Equation 5-2.

$$\tau_{wL} = f_L \frac{\rho_L\, v_{sL}^2}{2} \tag{5-3}$$

4. Determine pressure drop from Equation 5-4. The equation was obtained by adding the momentum equation of liquid for the gas core

$$-\frac{dp}{dL} A = g\left(A_L \rho_L + A_g \rho_g\right) \sin\theta + \tau_{wL} S_L \tag{5-4}$$

5. Determine the interface shear stress using the momentum equation for the liquid or the gas core
6. Calculate the interface friction factor

$$f_i = \frac{2\tau_i}{\rho_g v_g^2} \quad 5\text{-}5$$

where $v_g = v_{sg} \frac{A}{(1-A_L)}$

7. Plot the relation interfacial friction factor given in terms of a dimensionless parameter ***I*** against liquid holdup (H_L)

$$I = \frac{f_i}{\sin\theta\, f_g} \quad 5\text{-}6$$

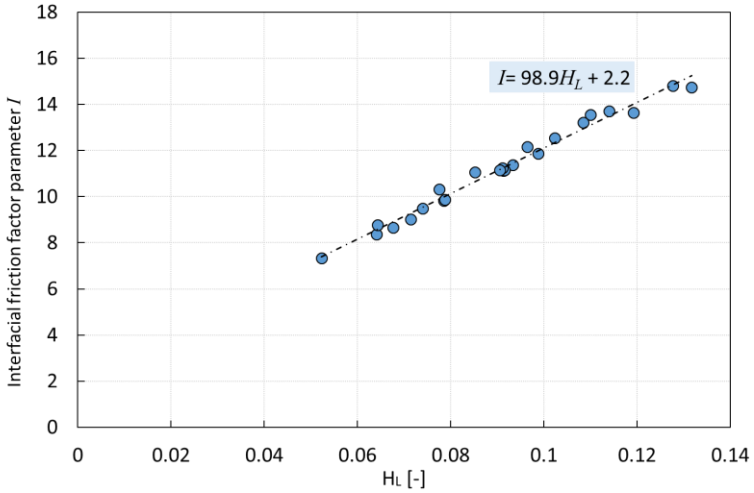

Fig. 5-3 Interfacial friction factor relationship with the liquid holdup estimated from Paz (1994) data

Fig. 5-4 presents the comparison of the interfacial friction factor estimated from the experimental data of Paz (1994) using the proposed Equation 3-10, Wallis (1969), Fore et al. (2000) (Equation 1-3) and Shekhar et al. (2017) (Equation 1-9). A scenario was also created in OLGA 7.3 to replicate the experimental condition used by Paz (1994). The interfacial friction factor was back-calculated from the pressure gradient.

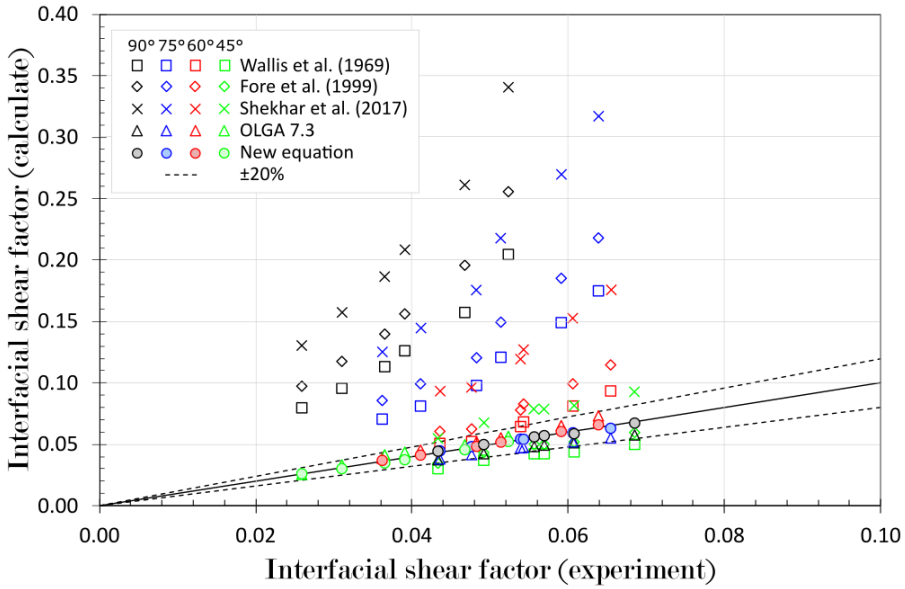

Fig. 5-4 Comparison of interfacial friction factor estimated from experimental Paz (1994) data with Wallis (1969), Fore et al. (2000), Shekhar et al. (2017) and OLGA prediction values of interfacial friction factor

It can be seen that the equations proposed by Wallis (1969), Fore et al. (2000) and Shekhar et al. (2017) overestimate the interfacial friction factor for inclinations above 45°. OLGA, however, predicted values close to the experimental estimation, as do the new equation predictions.